Supporting Information

Amorphous heterojunction and fluoride-induced effects enable a F-Ni(OH)$_2$/Ni-B electrocatalyst for efficient and stable alkaline freshwater/seawater hydrogen evolution at a high current density

Shenyi Chen[a], Haoming Chu[a], Ziyin Xie[a], Lihui Dong[a,b], Bin Li[a,b], Minguang Fan[a], Huibing He[a], and Zhengjun Chen[a*]

[a]Guangxi Key Laboratory of Electrochemical Energy Materials, School of Chemistry and Chemical Engineering, Guangxi University, Nanning 530004, PR China

[b]State Key Laboratory of Featured Metal Materials and Life-cycle Safety for Composite Structures, Guangxi University, Nanning 530004, PR. China

Corresponding Author

*E-mail address: zjchen@gxu.edu.cn (Z. Chen).

Experimental Section

Materials and Chemicals

Nickel foam (NF, ≥99%, ~1.8 mm in thickness, ~600 g m^{-2} in area density, Kunshan Jiayisheng Electronic Co., Ltd), hydrochloric acid (HCl, 36−38%, Chengdu Kelong Chemical Co., Ltd), Zinc nitrate hexahydrate ($Zn(NO_3)_2 \cdot 6H_2O$, 99%, Chengdu Kelong Chemical Co., Ltd), sodium chloride (NaCl, 99.5%, Shanghai Aladdin Biochemical Technology Co., Ltd), nickel chloride hexahydrate ($NiCl_2 \cdot 6H_2O$, 99%, Shanghai Macklin Biochemical Technology Co., Ltd), dimethylamino borane (DMAB, 97%, Shanghai Titan Scientific Co., Ltd), sodium succinate ($C_4H_4Na_2O_4$, 99%, Bide Pharmatech Co., Ltd), hexamethylene tetramine ($C_6H_{12}N_4$, 99%, Guangdong Guanghua Sci-Tech Co., Ltd), sodium fluoride (NaF, 98%, Guangdong Guanghua Sci-Tech Co., Ltd),potassium fluoride (KF, ≥99%, Shanghai Titan Scientific Co., Ltd), and potassium hydroxide (KOH, 85%, Chengdu Kelong Chemical Co., Ltd) were purchased and used directly.

Materials Characterization

The catalyst samples were characterized by field-emission scanning electron microscopy (FE-SEM, Hitachi, SU8220), X-ray diffraction (XRD, Bruker, D8 Discover, Cu Kα radiation), X-ray photoelectron spectroscopy (XPS, Thermo Fisher Scientific, ESCALAB 250XI+), transmission electron microscopy (TEM, FEI, Talos F200s) and Raman spectroscopy (Horiba, LabRAM HR Evolution). The high-resolution transmission electron microscopy (HRTEM) image was analyzed by Gatan digital micrograph software (Gatan, Inc.). The XPS peak positions were calibrated to the C 1s line (at 284.8 eV) of adventitious hydrocarbon.

Electrochemical Measurements

The electrochemical properties of catalysts were evaluated by a three-electrode system on the CHI660E and CHI1140C workstation with the catalyst as the working electrode (1×1 cm^2 geometric surface area), graphite rod as the counter electrode, and

Hg/HgO electrode (in 1M KOH) as the reference electrode. All potentials are expressed as relative potentials to reversible hydrogen electrode (RHE) according to the formula below:

$$E(RHE) = E(Hg/HgO) + 0.059 \times pH + 0.098$$

The linear sweep voltammetry (LSV) with a scan rate of 1 mV s^{-1} was utilized to capture the polarization curve. A 90% iR compensation was applied to all potentials according to the formula below:

$$E(corrected) = E(uncorrected) - iR$$

Electrochemical Impedance Spectroscopy (EIS) was conducted at open circuit to calculate the charge-transfer resistance (R_{ct}). The frequency range and AC amplitude were adjusted to 0.1 MHz ~ 0.01 Hz and 5 mV, respectively. At an open-circuit potential, Cyclic voltammetry (CV) with different scan rate (20 ~ 100 mV s^{-1}) was used to examine the electrochemical active surface area (ECSA). Double-layer capacitance of the catalyst (C_{dl}) is estimated by calculating the current difference when the scan rate increases. The linear slope is twice that of the electric double-layer capacitor C_{dl}. The Faraday efficiency (FE) is determined by dividing the actual H_2 production by the theoretical H_2 production, where the actual H_2 production can be obtained by H_2O drainage method. The chronoamperometry (CP) method is employed to assess the stability of catalysts.

Supporting Figures

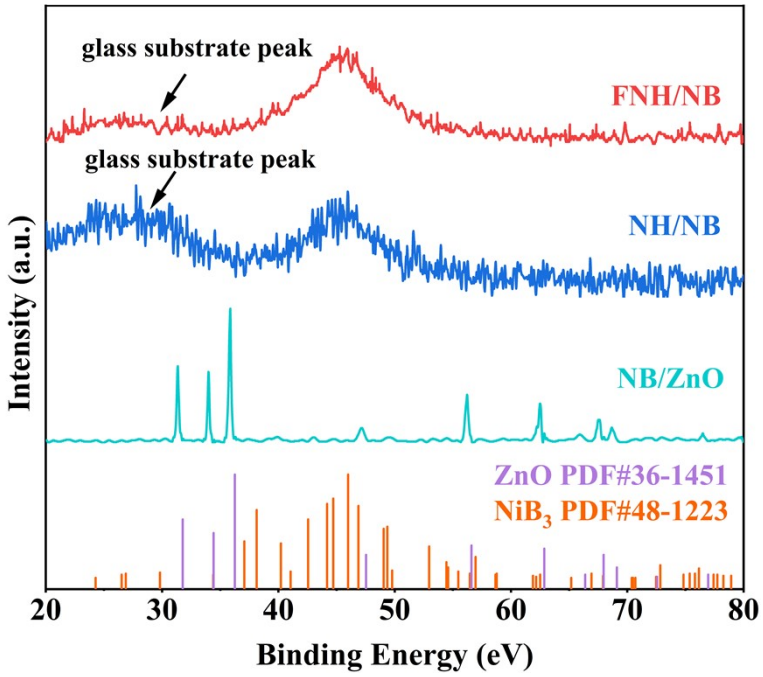

Fig. S1. XRD patterns of a series of catalysts scrapped from Ni foam

Table S1. EIS fitting data of a series of catalysts in 1.0 M KOH

Catalyst	R_s (Ω)	R_{ct} (Ω)	R_{ct} (Error)	R_{ct} (Error%)
FNH/NB	1.259	1.593	0.0282	1.7680
NH/NB	1.321	2.134	0.0255	1.3601
FNH	1.367	117.5	1.3425	1.1426
NB	1.569	64.23	2.6496	4.1252

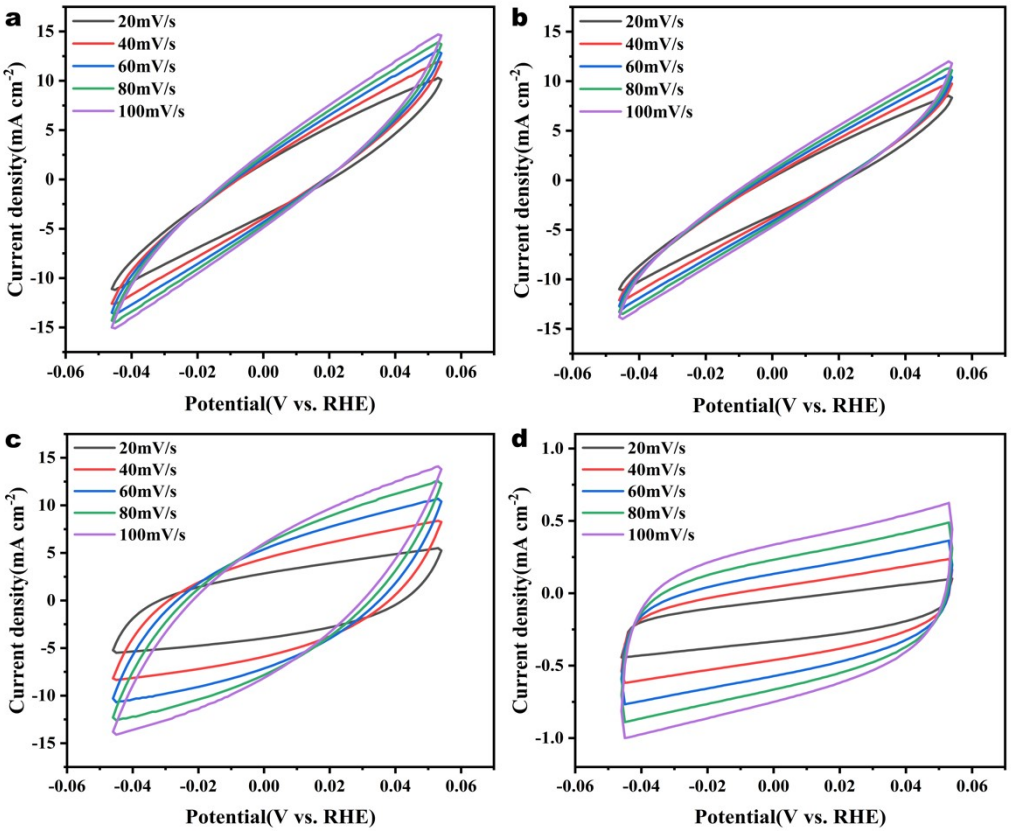

Fig. S2. CV curves of electrocatalysts obtained at different scaning rates in 1.0 M KOH: (a) FNH/NB; (b) NH/NB; (c) NB; (d) FNH.

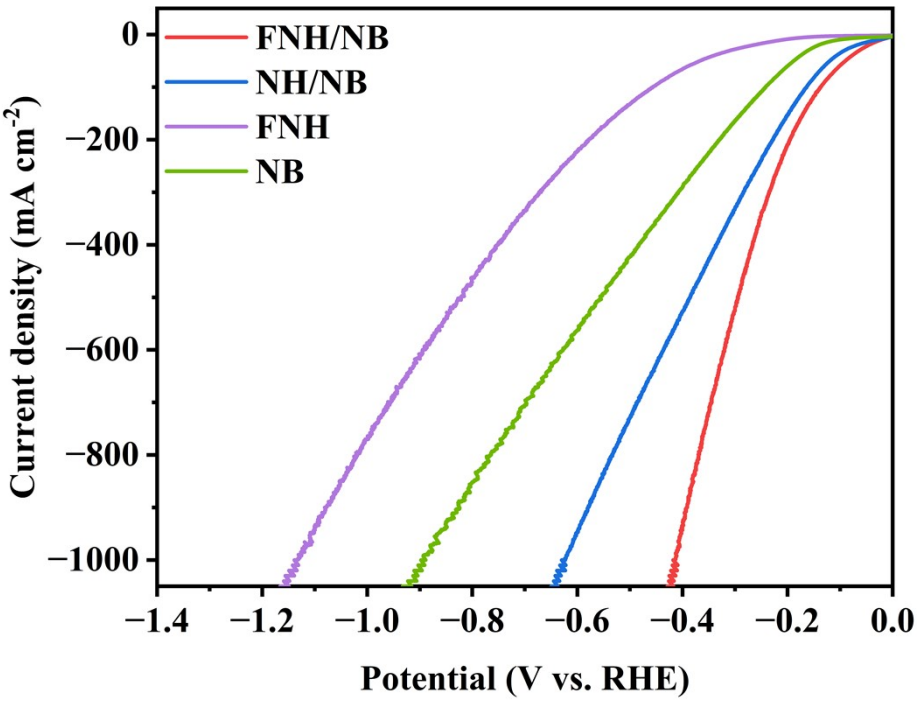

Fig. S3. HER polarization curves of FNH/NB and the series catalysts in real alkaline seawater (1.0 M KOH + seawater).

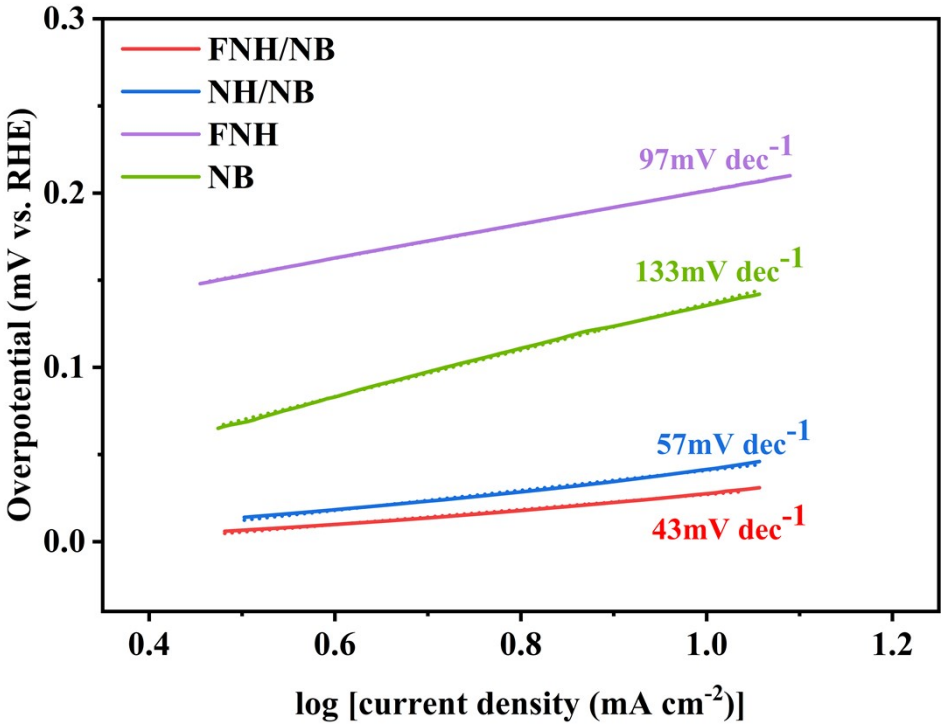

Fig. S4. Tafel plots of the serious catalysts in simulated alkaline seawater (1.0 M KOH + 0.5 M NaCl).

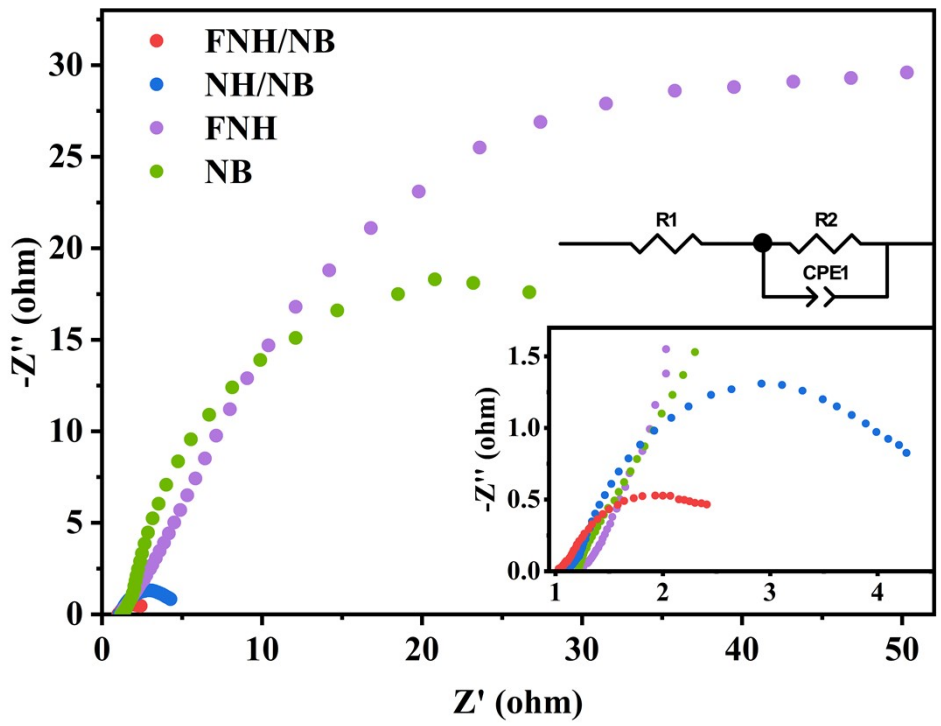

Fig. S5. EIS Nyquist plots of a series of catalysts in simulated alkaline seawater (1.0 M KOH + 0.5 M NaCl).

Table S2. EIS fitting data of a series of catalysts in simulated alkaline seawater (1.0 M KOH + 0.5 M NaCl).

Catalyst	R_s (Ω)	R_{ct} (Ω)	R_{ct} (Error)	R_{ct} (Error%)
FNH/NB	1.018	1.758	0.0180	1.0240
NH/NB	1.136	3.601	0.1355	0.6933
FNH	1.237	119.3	2.5146	2.1077
NB	1.284	53.30	1.8209	3.4163

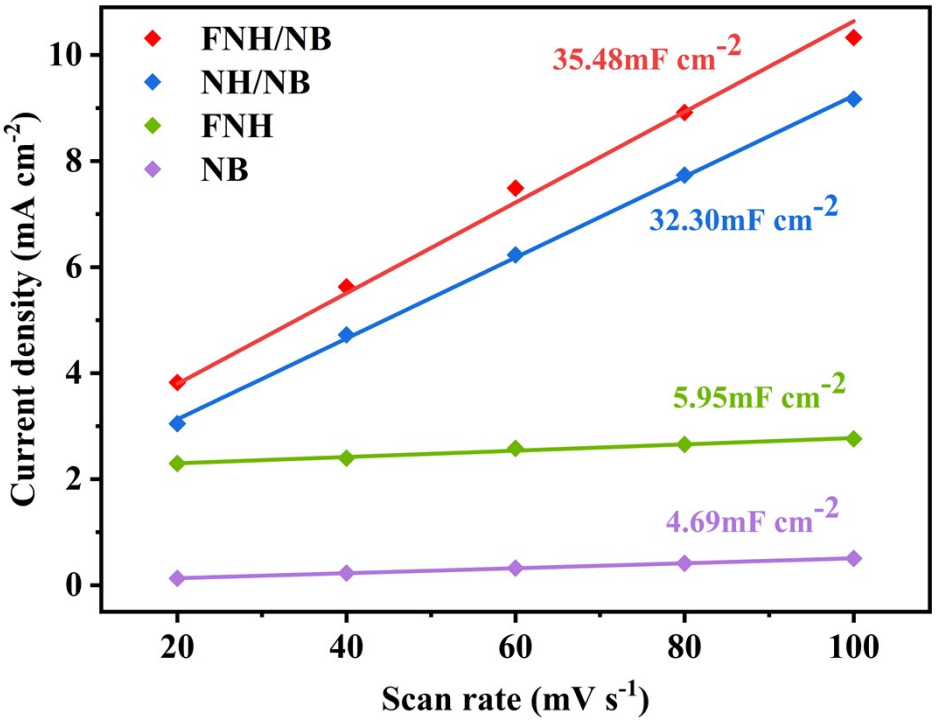

Fig. S6. C_{dl} values of a series of catalysts in simulated alkaline seawater (1.0 M KOH + 0.5 M NaCl).

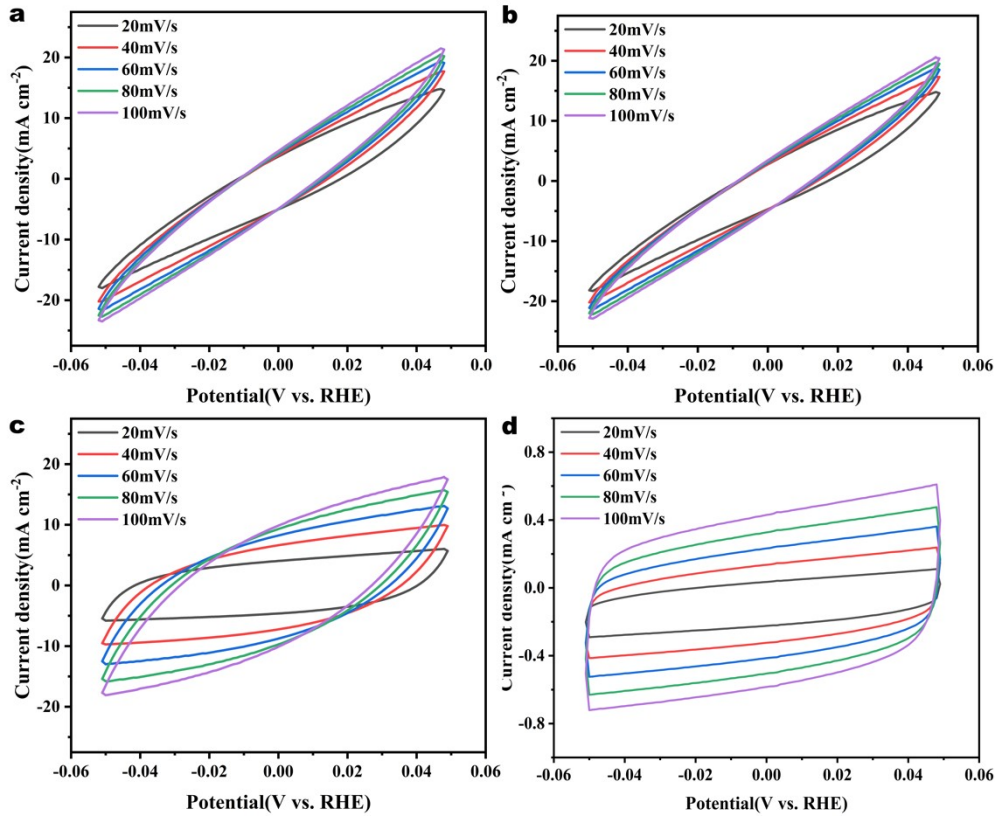

Fig. S7. CV curves of electrocatalysts obtained at different scaning rates in simulated alkaline seawater (1.0 M KOH + 0.5 M NaCl): (a) FNH/NB; (b) NH/NB; (c) NB; (d) FNH.

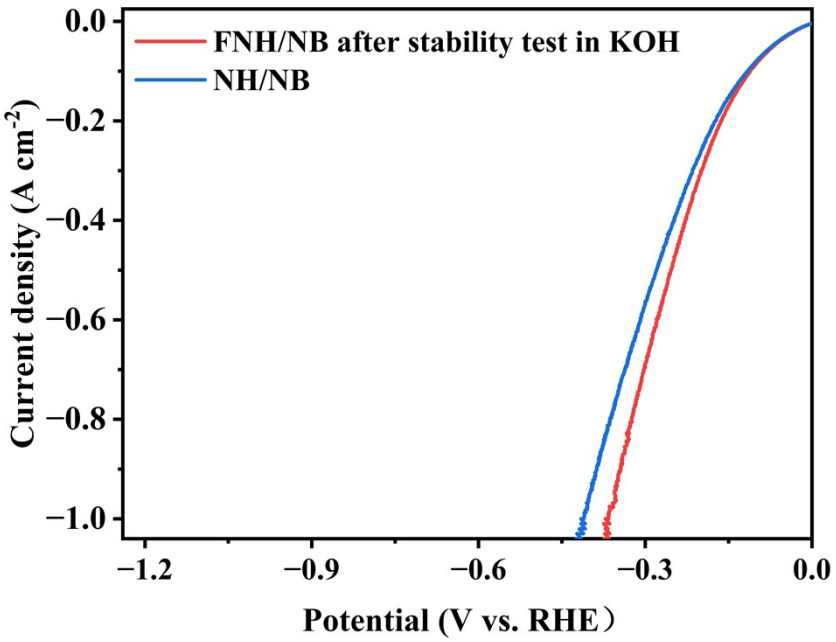

Fig. S8. LSV curves comparation of NH/NB and FNH/NB after stability test in 1.0 M KOH.

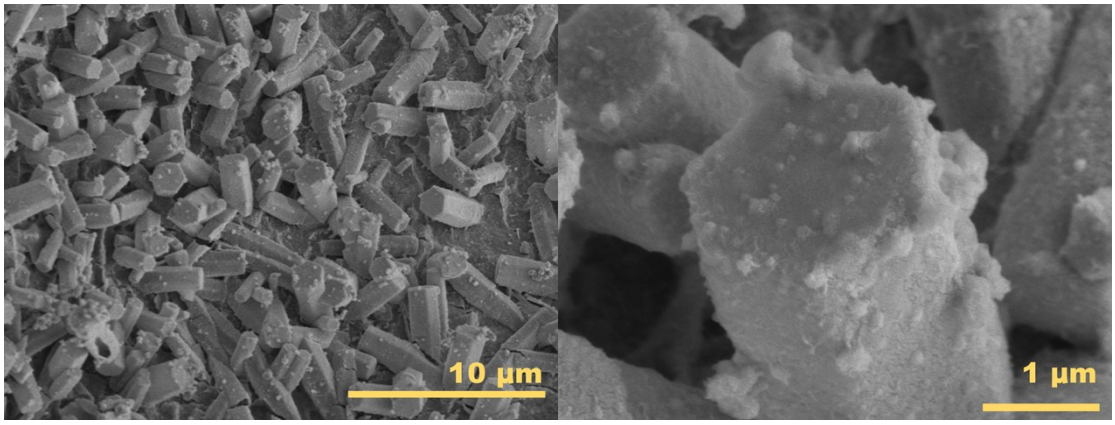

Fig. S9. SEM images of FNH/NB after stability test in 1.0 M KOH.

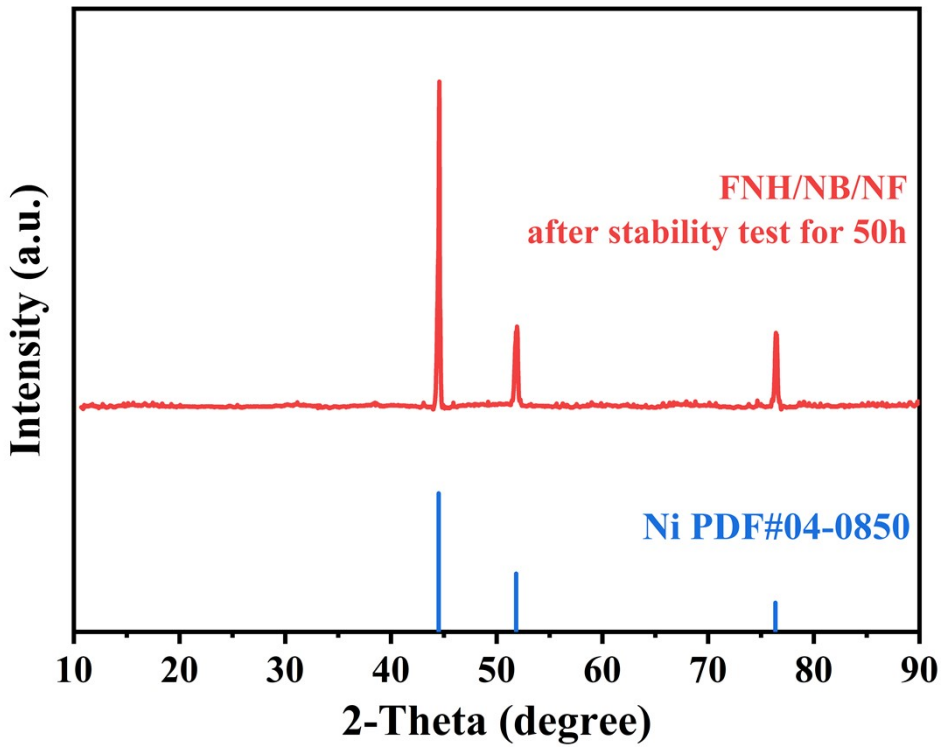

Fig. S10. XRD pattern of FNH/NB after stability test in 1.0 M KOH.

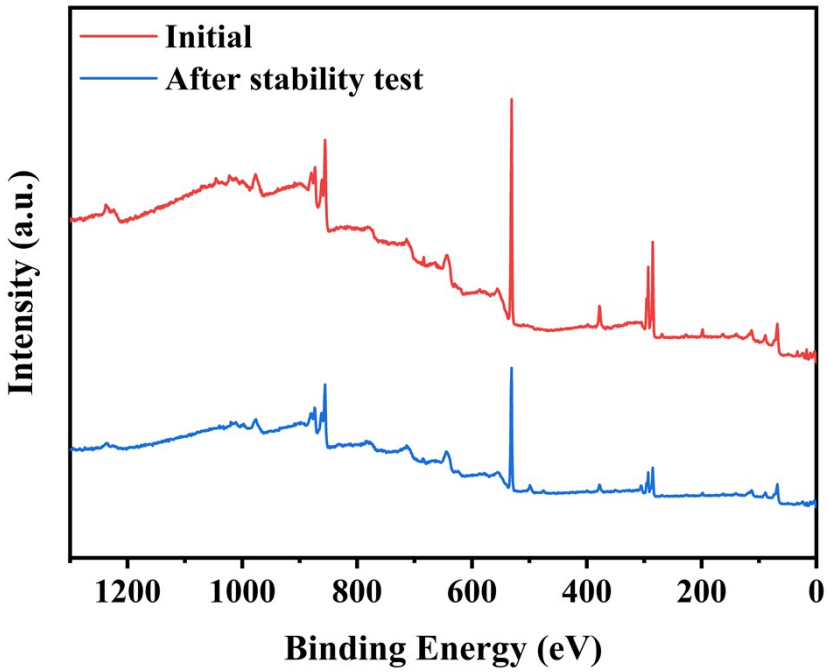

Fig. S11. XPS full spectra of FNH/NB after stability test in 1.0 M KOH.

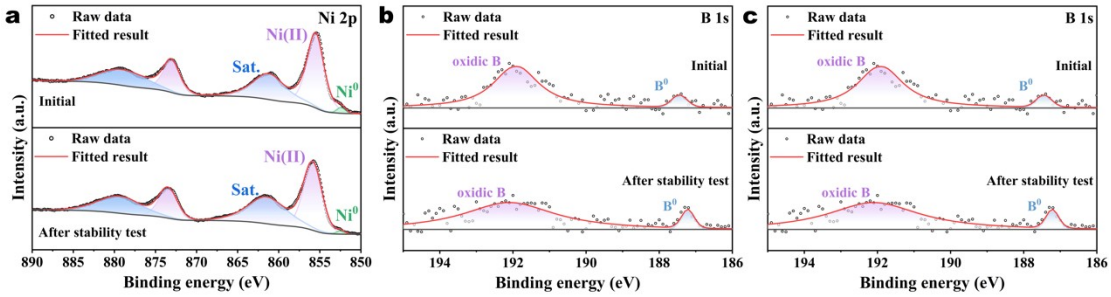

Fig. S12. XPS spectra of FNH/NB after stability test in 1.0 M KOH. (a) Ni 2p, (b) B 1s, and (c) F 1s

Table S3. Relative content of elements (atomic%) in FNH/NB analysed by XPS before and after stability test for 50 h in 1.0 M KOH.

Element	Before stability test		After stability test	
	raw data	Remove C element	raw data	Remove C element
Ni	12.72%	22.60%	15.28%	22.61%
B	1.17%	2.08%	0.81%	1.20%
O	41.75%	74.19%	50.63%	74.93%
F	0.63%	1.12%	0.85%	1.26%
C	43.73%	-	32.43%	-

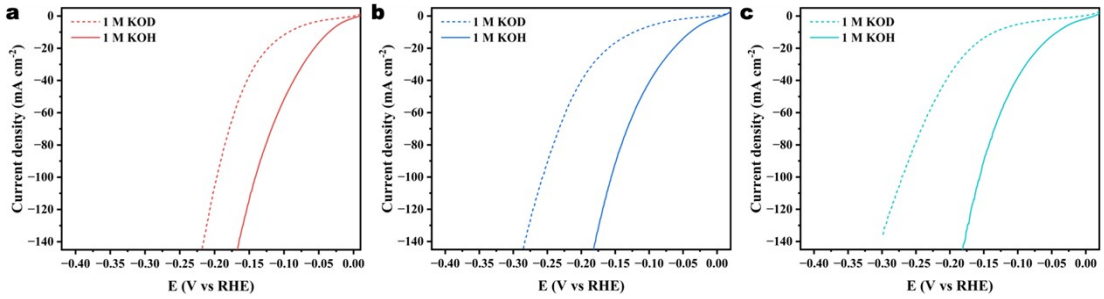

Fig. S13. Polarization curves of (a) FNH/NB, (b) NH/NB and (c) NB catalysts in 1.0 M KOH and 1.0 M KOD solutions.

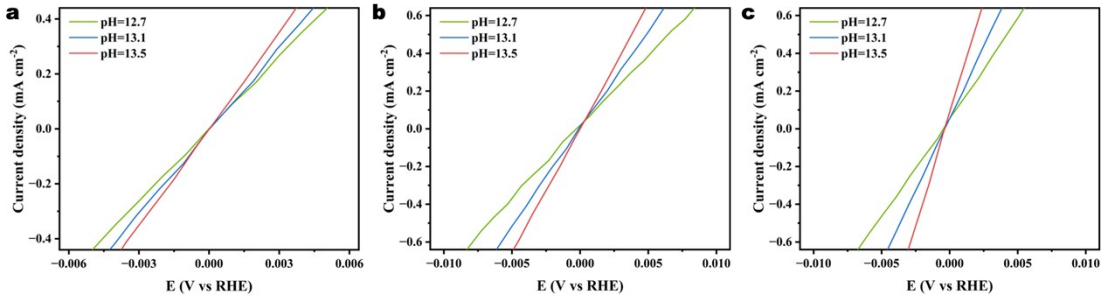

Fig. S14. Micropolarization curves of (a) FNH/NB, (b) NH/NB and (c) NB at different pH conditions.

Table S4. Summary of HER performance of recently reported catalysts in literatures.

Catalyst	Electrolyte	Current density ($mA \cdot cm^{-2}$)	Overpotential (mV)	Ref.
$Ni(OH)_2$@CuS	1.0 M KOH	10	95	[1]
a/a Ni–P/$Ni(OH)_2$	1.0 M KOH	10	54.7	[2]
Zn-VO_x-Co	1.0 M KOH	10	50	[3]
etched-NiPB@MS	1.0 M KOH	100	76	[4]
Co_2B/MoB_2	1.0 M KOH	500	304	[5]
$Ni(OH)_2$–$NiMoO_x$/NF	1.0 M KOH	10	36	[6]
Ni_xB/f-MWCNT	1.0 M KOH	10	116	[7]
Co−Mo−B/$CoMoO_{4-x}$/CF	1.0 M KOH	10	55	[8]
NiB/Ni	1.0 M KOH	10	78.2	[9]
Co-B/Ni	1.0 M KOH	10	70	[10]
Ni-ZIF/Ni-B@NF	1.0 M KOH	10	67	[11]
Co–Ni–B@NF	1.0 M KOH	10	205	[12]
NiCo/V_2O_3/C	1.0 M KOH	10 1000	23 396	[13]
N–MoO_2/Cu	1.0 M KOH	10 1000	40 363	[14]
A-NiCo LDH/NF	1.0 M KOH	100 1000	151 381	[15]
$NiCoS_x$@CoCH NAs/NF	1.0 M KOH	10 1000	55 438	[16]
Mn-Ni_2P/Fe_2P	1.0 M KOH	10 1000	90 405	[17]
FNH/NiB	**1.0 M KOH**	**10** **1000**	**23** **293**	**This work**

Reference

1. S. Q. Liu, H. R. Wen, Y. Guo, Y.-W. Zhu, X. Z. Fu, R. Sun and C. P. Wong, Amorphous $Ni(OH)_2$ encounter with crystalline CuS in hollow spheres: A mesoporous nano-shelled heterostructure for hydrogen evolution electrocatalysis, *Nano Energy*, 2018, **44**, 7–14.
2. F. Zhao, H. Liu, H. Zhu, X. Jiang, L. Zhu, W. Li and H. Chen, Amorphous/amorphous Ni–P/$Ni(OH)_2$ heterostructure nanotubes for an efficient alkaline hydrogen evolution reaction, *J. Mater. Chem. A*, 2021, **9**, 10169–10179.
3. M. Chen, J. Liu, N. Kitiphatpiboon, X. Li, J. Wang, X. Hao, A. Abudula, Y. Ma and G. Guan, Zn-VO_x-Co nanosheets with amorphous/crystalline heterostructure for highly efficient hydrogen evolution reaction, *Chem. Eng. J.*, 2022, **432**, 134329.
4. J. Zhang, Q. Wu, J. Song, C. Xu, S. Chen and Y. Guo, 3D transition metal boride monolithic electrode for industrial hectoampere-level current anion exchange membrane water electrolysis, *Nano Energy*, 2024, **128**, 109923.
5. X. Liu, Y. Yao, W. Li, Y. Zhang, Z. Liu, H. Yin and D. Wang, Molten-salt electrochemical preparation of Co_2B/MoB_2 heterostructured nanoclusters for boosted pH-universal hydrogen evolution, *Small*, 2024, **20**, 2308549.
6. Z. Dong, F. Lin, Y. Yao and L. Jiao, Crystalline $Ni(OH)_2$/amorphous $NiMoO_x$ mixed-catalyst with Pt-like performance for hydrogen production, *Adv. Energy Mater.*, 2019, **9**, 1902703.
7. X. Chen, Z. Yu, L. Wei, Z. Zhou, S. Zhai, J. Chen, Y. Wang, Q. Huang, H. E. Karahan, X. Liao and Y. Chen, Ultrathin nickel boride nanosheets anchored on functionalized carbon nanotubes as bifunctional electrocatalysts for overall water splitting, *J. Mater. Chem. A*, 2019, **7**, 764–774.
8. Y. Ren, J. Wang, W. Hu, H. Wen, Y. Qiu, P. Tang, M. Chen and P. Wang, Hierarchical nanostructured Co–Mo–B/$CoMoO_{4-x}$ amorphous composite for the alkaline hydrogen evolution reaction, *ACS Appl. Mater. Interfaces*, 2021, **13**, 42605–42612.
9. R. Zhang, H. Liu, C. Wang, L. Wang, Y. Yang and Y. Guo, Electroless plating of transition metal boride with high boron content as superior HER electrocatalyst,

ChemCatChem, 2020, **12**, 3068–3075.

10. W. Hao, R. Wu, R. Zhang, Y. Ha, Z. Chen, L. Wang, Y. Yang, X. Ma, D. Sun, F. Fang and Y. Guo, Electroless plating of highly efficient bifunctional boride-based electrodes toward practical overall water splitting, *Adv. Energy Mater.*, 2018, **8**, 1801372.
11. H. Xu, B. Fei, G. Cai, Y. Ha, J. Liu, H. Jia, J. Zhang, M. Liu and R. Wu, Boronization-induced ultrathin 2D nanosheets with abundant crystalline–amorphous phase boundary supported on nickel foam toward efficient water splitting, *Adv. Energy Mater.*, 2020, **10**, 1902714.
12. N. Xu, G. Cao, Z. Chen, Q. Kang, H. Dai and P. Wang, Cobalt nickel boride as an active electrocatalyst for water splitting, *J. Mater. Chem. A*, 2017, **5**, 12379–12384.
13. D. Li, J. Wang, S. Wang, B. Chu, R. Li, B. Li, L. Dong, M. Fan and Z. Chen, An interface engineering induced hierarchical NiCo/V_2O_3/C Schottky heterojunction catalyst for large-current-density hydrogen evolution reaction, *J. Mater. Chem. A*, 2023, **11**, 23397–23404.
14. S. Wang, S. Chen, C. Wen, L. Dong, C. Tan, B. Li, M. Fan, H. He and Z. Chen, Nitrogen-doped MoO_2/Cu heterojunction electrocatalyst for highly efficient alkaline hydrogen evolution reaction, *Int. J. Hydrog. Energy*, 2024, **66**, 103–109.
15. H. Yang, Z. Chen, P. Guo, B. Fei and R. Wu, B-doping-induced amorphization of LDH for large-current-density hydrogen evolution reaction, *Appl. Catal. B Environ.*, 2020, **261**, 118240.
16. X. Zhang, R. Zheng, M. Jin, R. Shi, Z. Ai, A. Amini, Q. Lian, C. Cheng and S. Song, $NiCoS_x$@cobalt carbonate hydroxide obtained by surface sulfurization for efficient and stable hydrogen evolution at large current densities, *ACS Appl. Mater. Interfaces*, 2021, **13**, 35647–35656.
17. Y. Luo, P. Wang, G. Zhang, S. Wu, Z. Chen, H. Ranganathan, S. Sun and Z. Shi, Mn-doped nickel–iron phosphide heterointerface nanoflowers for efficient alkaline freshwater/seawater splitting at high current densities, *Chem. Eng. J.*, 2023, **454**, 140061.